# Properties and Potential for Application of Steel Reinforced Polymer (SRP) and Steel Reinforced Grout (SRG) Composites

**X. Huang[1], V. Birman[2], A. Nanni[1], and G. Tunis[3]**

## Abstract

The paper introduces steel reinforced polymer (SRP) and steel reinforced grout (SRG) composites that are considered for application in civil engineering for bridge and concrete buildings upgrade. These composites consist of steel cords formed by interwoven steel wires embedded within a polymer resin or cementitious grout matrix. The properties of SRP are evaluated experimentally and compared to micromechanical equations to determine a suitability of these equations for the prediction of material constants. The effectiveness of SRP is evaluated on existing structures (i.e., slab strips of a parking garage) while SRG performance is studied on laboratory-prepared large-scale reinforced concrete beams. It is shown that both composites significantly enhance the strength of the concrete members providing the first evidence of their suitability for practical applications concerned with upgrading the existing infrastructure. Improvements subsequent to the testing to both the cord design and fabric manufacturing process show even greater promise.

*Keywords:* Composites; Concrete; Mechanical properties; Repair; Steel cord, Steel reinforced grout; Steel reinforced polymer; Testing; Upgrade.

[1] Civil Engineering, University of Missouri – Rolla, Rolla, MO 65409

[2] Engineering Education Center in St. Louis, University of Missouri – Rolla, St. Louis, MO 63121

[3] Hardwire, LLC, Pocomoke City, MD 21851

## Introduction

Feasibility studies on the use of fiber reinforced polymer (FRP) composites for strengthening and new construction of concrete members date back to the beginning of the nineties. Different aspects of these applications of FRP composites are described in the published literature [1-9]. The main obstacles to a widespread use of FRP remain its relatively high cost and lack of confidence in long-term durability. In particular, the former factor, i.e. cost, is very important because of the scale of necessary repairs and upgrades of the existing civil infrastructure. For example, 180,000 bridges in the USA are considered deficient with the cost of repair or replacement estimated at $20 billion [9].

Steel reinforced polymers (SRP) are less expensive composites that are currently considered for numerous applications in civil engineering, such as bridge and building repair. Typically, these composites consist of steel wires forming cords that are assembled into a fabric and embedded within a polymeric matrix. A cross section of such cord photographed under a microscope is depicted in Fig. 1.

Performance of a composite material utilizing steel wires is controlled by the stress transfer between the wires and the matrix. A single high-strength wire may be deficient due to low interfacial shear strength and stiffness. This problem is solved in SRP by using twisted steel filaments forming the cord, as shown in Figs. 2 and 3. The rough surface of the cord provides a mechanical interlock with the matrix resulting in a system suitable for structural applications. As an example, the cord shown in Fig. 2 is produced by twisting one wire at a short lay length around 12 wires that are twisted in a long lay length. The warp wire provides additional surface roughness and tightens the cord enhancing its integrity. The cord shown in Fig. 3 consists of a two-wire strand twisted around a three-wire strand. Differently from the sample in Fig. 2, this cord has a more pronounced surface roughness distribution.

The stiffness and strength of composites utilizing the steel cords shown in Figs. 2 and 3 may differ due to a different cord surface geometry. In all cases, it is desirable to produce SRP where the failure of the cord under tension preempts its pullout. In experiments, both cords shown in Figs. 2 and 3 failed prior to pullout from typical polymeric matrices at a relatively short development length of only about 1in. This implies high quality of the interfacial mechanical interlock between the cords and matrix that is crucial for a successful use of SRP.

SRG composites are similar to their SRP counterparts, except for the polymer resin that is replaced with a cementitious grout. The grout that was found most suitable for the impregnation of the steel cord is a polymer-modified cementitious grout combined with a corrosion inhibitor.

Unidirectional cords can be held in place by knit yarns forming an appropriate pattern of fabric. The yarns control the spacing of the cords and as a result, the "net" behaves like a fabric that can be stretched or bent, without losing its integrity. A typical knit yarn material is polyester; a "net" consisting of the cords held by polyester yarns is shown in Fig. 4.

The addition of copper knit yarns results in the fabric capable of maintaining the spacing between steel cords, even under significant handling loads. In addition, such fabric has excellent electric conductivity. Copper wires used in this example had a diameter equal to 0.006 in. The copper wire is tied to the steel cords by the spiraling polyester knit thread, as shown in Fig. 5.

Post-testing enhancements have been made to the fabric making process that no longer require knitting of materials and simply bind the steel cords to a fiberglass scrim with adhesives. This allows for better control of cord density during the manufacturing process and makes possible the manufacture of any density fabric. The process also yields a 17% increase in the number of cords per inch and thus higher fabric properties. The new fabric lays flatter and straighter than the knitted fabrics and can be applied faster and easier.

Additionally, new cord designs have been created to optimize the compressive qualities and provide more balanced compressive and tensile properties.

SRP and SRG can be reliably used in practical applications only if their properties are known from experiments. Nevertheless, the validation of a micromechanical theory suitable for the prediction of these properties is essential for design purposes. A number of factors, such as rough cord-matrix interface, high porosity, and manufacturing defects, may interfere with the accuracy of a theory developed for conventional composites. Therefore, two essential issues that have to be addressed in experiments on a representative SRP (or SRG) specimen include determining the properties of the material and a comparison of these properties with one of the available micromechanical models.

Another important issue is bonding between SRP (or SRG) and the parent material (e.g., concrete substrate). The adhesive must be able to protect the integrity of the bond subject to environmental and mechanical loads. Finally, it is important to illustrate examples of successful reinforcement of structures by SRP (or SRG) validating the concept that unidirectional elements with the cords oriented in the load direction can improve the capacity of the member. The research outlined in this paper was conducted to prove the feasibility of SRP and SRG. Accordingly, the issues discussed above have been addressed in the course of this study.

**Experimental Analysis**

Steel cords employed in the present study had a diameter equal to 0.044 in and consisted of 13 filaments (Fig. 2). Three of these filaments had a diameter equal to 0.22 micron, nine filaments had 0.20-micron diameter, and one of them had a 0.15-micron diameter. Several different impregnating resins were considered, including Epon 828 + Hardener HT-386, M-Brace Saturant, SikaDur 330 and SikaTop 121. Epon 828 was used in the tests described in this paper.

1. Evaluation of Material Constants of SRP

Unidirectional SRP samples were tested in tension and compression using an MTS 880 testing machine. The specimens were premanufactured using compression molding into a plate, shipped to the laboratory, and cut to size by waterjet.

The matrix material used in the tested specimens was Epon 828 with Hardener HT-386. The properties of Epon 828 tested after curing at 200$^{o}$F for two hours are outlined in Table 1. These properties were used in the computations performed to compare micromechanical predictions for material properties with experimental data.

The specimens had geometrical dimensions as reported in Table 2 together with the direction of the load as compared to that of the cords. A photograph depicting the cross section of a typical specimen is shown in Fig. 6. The results of the tests are shown in Tables 3-7. In these tables, the subscripts "w," "c" and "cs" refer to steel wire, steel cord and SRP composite, respectively. The directions 1 and 2 refer to the longitudinal (along the cord) and transverse (perpendicular to the cord) directions. The material constants that are analyzed include the elastic moduli $(E_1, E_2)$, the shear modulus $(G_{12})$, and the Poisson ratios $(\nu_{12}, \nu_{21})$. In addition, the strength of the material $(F)$ is evaluated, both in tension and in compression, in the longitudinal and transverse directions.

The results of longitudinal tensile testing of five specimens are presented in Table 3. In particular, longitudinal tensile moduli of individual wires and the cord are shown in this table. Predictably, the modulus of the cord is smaller than that of wires, as a result of the twisting and matrix content in the cord (the latter is clearly visible in Fig. 1). The longitudinal modulus of SRP is much lower than the corresponding modulus of the cords. The variation in the stiffness of five tested specimens was not very large, except for the SLT1-1. The reason for this difference is evident from the comparison of the stiffness of the constituent wires of the specimens. Obviously, the specimen in question was manufactured using substandard steel wires, compared to its counterparts. The same conclusion follows from the comparison of the strength of wires used in SLT1-1 and

other specimens (except for SLT1-3). Accordingly, the results for SLT1-1 are discounted in the average values shown in the last row of the table.

As indicated in the Table 3, the specimen SLT1-3 failed at grips. Therefore, the failure stress obtained for this specimen is not included in the calculation of the strength of SRP. Accordingly, the average value in the last row of the table include the stiffness and Poisson ratio evaluated from the analysis of specimens SLT1-2 through 5 and the strength from the analysis of specimens SLT1-2, 4 and 5.

The results of longitudinal compressive tests are shown in Table 4. Notably, the stiffness (modulus) of SRP in compression is much higher than in tension. This is explained by a much higher compressive stiffness of the wires that constitute the cords (compare Tables 3 and 4). The results for compressive strength are not shown in Table 4 since the mode of failure observed in the experiments was cord buckling. Again, post-testing enhancements to the cord design have addressed the cord buckling failure by creating a structure that resists this type of failure by eliminating the deformations in the core filaments which result from the cord manufacturing process.

The results of transverse tension and transverse compression tests are collected in Tables 5 and 6. Predictably, the transverse stiffness and strength in tension are much lower than in compression. A significant difference in the Poisson ratios $\nu_{21}$ evaluated in transverse tests under tensile and compressive loads was also observed. Note that the ratio of the Poisson value in tension to its counterpart in compression is close to being inversely proportional to the ratio of the stiffness in tension to that in compression.

The in-plane shear modulus $G_{12}$ was obtained by combining the results from the tension tests in longitudinal and transverse directions with the results from the tests on coupons oriented at $45^{o}$ relative to the applied tensile load. The transformation equation for the stiffness of a lamina oriented at an angle $\theta$ relative to the applied load is

$$\frac{1}{E_\theta} = \frac{\cos^4\theta}{E_1} + \frac{\sin^4\theta}{E_2} + (\frac{1}{G_{12}} - \frac{2\nu_{12}}{E_1})\sin^2\theta\cos^2\theta \quad (1)$$

From this equation, the shear modulus can be obtained in the form $(\theta = 45^0)$:

$$G_{12} = \frac{1}{\frac{4}{E_{45}} - \frac{1}{E_1} - \frac{1}{E_2} + \frac{2\nu_{12}}{E_1}} \quad (2)$$

The results of these tests are shown in Table 7. Remarkably, the variation between three evaluated specimens was small.

## 2. Comparison of Experimental Results with Predictions Obtained by Micromechanical Theory

This comparison is needed to conclude whether it is possible to use micromechanical theories developed for conventional composites to predict the properties of SRP. The applicability of conventional micromechanics may be affected by a number of factors that include relatively large diameter of the cords, twisting of the wires in the cords, and even more importantly, the roughness of cord-matrix interface. Unavoidable porosity of SRP, particularly along the cord-matrix interface with its rough surface, may contribute to the inaccuracy of micromechanical relationships. In this paper, a comparison was made to the micromechanical theory developed based on the mechanics of materials [10]. The relationships employed in this theory are outlined below.

The assumptions regarding the material phases constituting the composite that are utilized in the micromechanical theory based on mechanics of materials are:

1. Both fibers and matrix are linearly elastic isotropic materials.
2. Fibers are uniformly distributed in the matrix.
3. Fibers are perfectly aligned.

4. There is perfect bonding between fibers and matrix.
5. The composite lamina is free of voids.

Based on these assumptions, the longitudinal modulus is calculated by the rule of mixtures as

$$E_1 = E_f V_f + E_m V_m \tag{3}$$

where $E_1$ is a longitudinal elastic modulus of the composite material, $E_f$ is the elastic modulus of the fibers, $V_f$ is the fiber volume fraction (equal to 0.27 in this case), $E_m$ is the elastic modulus of matrix (equal to 0.44 Msi in this case), and $V_m$ is the volume fracture of matrix. The porosity was not measured in the experiments and accordingly, the matrix volume fraction was assumed equal to 0.73. It is necessary to emphasize that the "fibers" referred to in this section represent steel wires, rather than the cords since the latter include the pockets of matrix. Accordingly, the properties of the wires should be employed in the corresponding equations.

The transverse elastic modulus in the direction perpendicular to the fibers can be obtained from the inverse rule of mixtures:

$$E_2 = \frac{E_f E_m}{E_f V_m + E_m V_f} \tag{4}$$

The Poisson ratios are determined from

$$\nu_{12} = \nu_f V_f + \nu_m V_m$$

$$\nu_{21} = \frac{E_2}{E_1}\nu_{12} \tag{5}$$

where $\nu_f$ is the fiber (steel wires) Poisson's ratio that was equal to 0.30 and $\nu_m$ is Poisson's ratio of matrix.

The in-plane shear modulus is obtained from

$$G_{12} = \frac{G_f G_m}{G_f V_m + G_m V_f} \tag{6}$$

where $G_f$ and $G_m$ are the shear moduli of the fiber and matrix materials, respectively.

It is known that the formulae of mechanics of materials are often inaccurate for the transverse modulus of elasticity and for the in-plane shear modulus. The so-called improved mechanics of materials approach [10] results in the following equations for these material constants:

$$E_2 = \frac{E_m}{1-\sqrt{V_f}\,(1-E_m/E_f)}$$

$$G_{12} = \frac{G_m}{1-\sqrt{V_f}\,(1-G_m/G_f)} \tag{7}$$

The comparison between experimental results and the properties predicted by micromechanics based on mechanics of materials is presented in Table 8. As follows from this table, theoretical predictions for the tensile and compressive longitudinal modulus of elasticity and for the in-plane shear modulus are in good agreement with experimental data. The agreement for tensile transverse modulus of elasticity and for both Poisson ratios is less satisfactory. However, even these material constants can be adequately predicted by the micromechanical theory considered in the paper. However, the compressive modulus could not be obtained from micromechanics. Notably, tensile transverse and in-plane shear moduli should be calculated by the improved mechanics of materials, i.e. equations (7).

The main application of SRP is envisioned in the situations where these composites are subject to longitudinal tension. Accordingly, it is also important to compare the longitudinal strengths available from the experiments (122 ksi) to the theoretically predicted value. The latter value is obtained by the rule of mixtures:

$$F_{cs} = F_f V_f + F_m V_m \tag{8}$$

The substitution of the strengths of wire and matrix yields the value of 126 ksi that is remarkably close to the experimental result. This figure can be further improved by increasing the packing density of the cords (available with the new manufacturing process) and by moving to one of the higher property cords.

## 3. Experimental Evaluation of Flexural Properties of SRP

The flexural strength of SRP was evaluated from a three-point bending test designed according to ASTM D 790 [11]. Accordingly, detailed description of the tests is omitted since it can be found in this standard.

The size of the specimens used in the flexural tests is shown in Table 9. A typical load-midspan deflection curve for one of the specimens is shown in Fig. 7. The modes of failure were rupture on the tensile surface of the specimens and fiber microbuckling on their compressed surface. The effect of these modes of failure, particularly fiber microbuckling and related softening of the response, is clearly observed in Fig. 7.

Following [11], the maximum flexural stress in the outer fibers at the midspan of the specimen was calculated from

$$\sigma_f = \frac{3PL}{2bd^2} \tag{9}$$

where $P$ is the load, $L$ is the span, and $b$ and $d$ are the width and the depth of the beam, respectively.

In the case of large span-to-depth ratios, such as in specimens SF4 and SF5, the moment at the midspan is affected by relatively large deflections. Accordingly, (9) is modified to account for these effects:

$$\sigma_f = \frac{3PL}{2bd^2}\left[1+6\left(\frac{D}{L}\right)^2-4\left(\frac{d}{L}\right)\left(\frac{D}{L}\right)\right] \tag{10}$$

The test results and the corresponding maximum flexural stress (flexural strength) of the tested specimens are shown in Table 10. Note that the difference between flexural strengths found for five specimens was small.

## 4. Field Tests of SRP and FRP Reinforced Concrete Beams

The tests on the effectiveness of SRP reinforcement in concrete beams of existing structures were conducted in Clayton, Missouri. Four strips were cut out of the deck of a parking garage. Each strip (beam) consisting of three equal spans had the overall length of 26 feet and a rectangular cross section that was 24 inches deep and 6 inches wide. The beams were strengthened as follows:

Beam 1: No strengthening;
Beam 2: Two plies of carbon FRP (CFRP) reinforcement in the positive moment region;
Beam 3: Two plies of CFRP reinforcement in both the positive and negative moment regions;
Beam 4: One ply of SRP reinforcement in negative moment region and two plies of CFRP reinforcement in positive moment region.

The width of all CFRP and SRP reinforcements was 18 inches. The strength, elastic modulus and thickness of CFRP components used in the test were 550 ksi, 33000 ksi and

0.0065 inch per ply, respectively. The SRP components had a density of 12 cords per inch of the width; the area of one cord's cross-section was 0.000615 square inch. As indicated above, the strength and elastic modulus of SRP are 447 ksi and 29900 ksi, respectively. With reference to Fig. 8, the positive moment region refers to the bottom central portion of the left span, where Load 1 was applied; and the negative moment region refers to the top of second support where the maximum negative moment occurred.

As show in Fig. 8, a two-point-load test set up was used. Two jacks were used to apply load. One was placed at the middle of left span (Load 1) and the other placed at the middle of the central span (Load 2). During the test, Load 1 was kept equal twice the value of Load 2.

The load-deflection relationships obtained for the four beams are shown in Fig. 9. Both FRP and SRP reinforcements significantly increase the ultimate capacity of the beams (this increase exceeded 100% for the three strengthened beams). The flexural stiffness of the beams was also significantly improved. Table 11 compares the nominal moment ($M_n$) computed for the benchmark and the SRP strengthened beam using conventional reinforced concrete theory and that obtained experimentally (Mu). The prediction is rather satisfactory also considering the fact that failure for the strengthened member was in the positive moment region of the first span, rather than on top of the internal support for the benchmark.

An important issue that has to be considered is related to bond integrity between SRP or SRG reinforcements and concrete beams. This was addressed by testing the bond between several SRP specimens with various bond lengths (2, 4 and 6 inches) and concrete. The concrete surfaces were sand blasted prior to bonding to reduce surface roughness. Subsequently, a laser profilometer was used to measure the surface roughness.

Tested specimens failed along the concrete-SRP interface. The average bond strength was found equal to 1.93 MPa. Such strength is considered sufficient for the majority of applications utilizing SRP reinforcements.

## 5. Testing SRG Strengthened Reinforced Concrete Beams

SRG represents an alternative to SRP where a resin matrix material is replaced with cementitious grout. The feasibility of SRG strengthening for concrete beams was experimentally investigated by comparing the performance of three reinforced concrete beams subject to four-point bending. The cross section and geometry of the beams are shown in Fig. 10 together with the internal steel reinforcement. The yield point of reinforcing bars and the concrete compressive strength were equal to 80 ksi and 6.3 ksi, respectively.

One beam was used as the control specimen (no strengthening), one beam was strengthened with SRP and one with SRG. The latter used SikaTop 121 as the impregnating grout. This is a two component, polymer-modified, leveling and pore sealing grout. An advantage of this material is the presence of FerroGard 901 penetrating corrosion inhibitor. SicaTop 121 is known for excellent adhesion to concrete and mortar surfaces and high flexural and compressive strength. In addition, SicaTop 121 possesses good freeze-thaw durability, high resistance to deicing salts, compatibility with thermal expansion coefficients of concrete, non-flammability, and non-toxicity. Note that the resistance to deicing salts makes SicaTop 121 particularly attractive since these salts are responsible for damage to concrete bridge structures, as discussed in [9].

The load-midspan deflection relationships for three beams are shown in Fig. 11. The load and deflection corresponding to the initiation of cracking in concrete are clearly observed for all three beams. Prior to cracking, the beams have an almost identical stiffness. A slightly higher stiffness of SRP and SRG-strengthened beams can be explained by the contribution of SRP and SRG elements. The increases in the yield stress for SRP and SRG over the yield stress of the control beam were 33% and 7%,

respectively. The ultimate loads of the beams were 67 kips (SRP), 62 kips (SRG), and 51 kips (control beam). The ultimate failure occurred at midspan of the beams. The failure was brittle and controlled by peeling of the strengthening shown in Fig. 12. Based on experimental results, it is apparent that SRG, even thought less effective than SRP, has good potential in structural applications.

## Conclusions

The paper presents the results of an experimental study concerned with the feasibility of using steel reinforced plastics (SRP) and steel reinforced grout (SRG) for strengthening civil structures. The study yielded the following conclusions.

- SRP and SRG can be easily and economically manufactured offering great potential for strengthening of concrete bridges and buildings. SRP and SRG elements can be easily and reliably bonded to concrete structures.
- The properties of SRP can be accurately predicted by mechanics of materials using micromechanics models. These properties include the tensile and compressive moduli in the direction of the steel cords, the in-plane shear modulus, and the tensile axial strength. The transverse tensile modulus and the Poisson ratios can also be estimated analytically, though with a smaller accuracy. However, the transverse modulus corresponding to compression could not be accurately determined from micromechanics.
- The ultimate strength tested in–situ of a reinforced concrete flexural member obtained by saw cutting an existing parking garage floor was more than doubled when strengthening with SRP and CFRP composites.
- In laboratory tests, the strength increase in a reinforced concrete beam strengthened with SRP and SRG was higher than 30 and 20%, respectively.

Based on these results, it is apparent that both SRP and SRG can be successfully used for repairs and retrofit of the built infrastructure and potentially in new construction.

**Acknowledgements:**

This work was conducted with partial support from the National Science Foundation Industry/ University Research Center on Repair of Buildings and Bridges with Composites ($RB^2C$) based at the University of Missouri-Rolla.

**References**

1. Iyer SL and Sen R, editors. Advanced Composite Materials in Civil Engineering Structures. Proc., American Society of Civil Engineers, New York, NY, ASCE, 1991. 443 pages.
2. White TD, editor. Composite Materials and Structural Plastics in Civil Engineering Construction. Proc., American Society of Civil Engineers, New York, NY, ASCE, 1992. p. 532-718.
3. Neale KW and Labossiere P, editors. Advanced Composite Materials in Bridges and Structures. Proc. Canadian Society for Civil Engineering, Montreal, Canada, 1992. 705 pages.
4. Nanni A. Fiber-Reinforced-Plastic (FRP) Reinforcement for Concrete Structures: Properties and Applications. In: Developments in Civil Engineering 1993; 42. 450 pages.
5. Nanni A and Dolan CW, editors. FRP Reinforcement for Concrete Structures. Proc. American Concrete Institute, (ASCI SP-138), Detroit, MI, Amer. Concrete Institute, 1993. 977 pages.
6. El-Badry M, editor. Advanced Composite Materials in Bridges and Structures. Proc. ACMBS-II, Montreal, Canada, 1996. 1027 pages.
7. Dolan CW, Rizkalla SH and Nanni A, editors. Proc. Fourth International Symposium on Fiber Reinforced Polymer Reinforcement for Reinforced Concrete Structures (FRPRCS-4), SP-188. American Concrete Institute, Farmington Hills, MI, 1999. 1182 pages.
8. Meier U. Advanced solutions with composites in construction. Proc. International Conference in Composites in Construction (CCC2001), Porto, Portugal, October 10-12, p. 3-7.

9. Alampalli S, O'Connor J and Yannotti AP. Fiber reinforced polymer composites for the superstructure of a short-span rural bridge. Composite Structures 2002; 58: 21-27.
10. Gibson, RF. Principles of Composite Material Mechanics. McGraw-Hill, Inc., New York, NY, 1994.
11. ASTM Standard D 790, Standard Test Methods for Flexural Properties of Unreinforced and Reinforced Plastics and Electrical Insulating Materials. Current edition approved on April 10, 2002.

## Figure Captions

Fig. 1. Cross-section of a steel cord showing individual wires and pockets of resin (SRP)

Fig. 2. Steel cord with 12 wires wrapped by one wire

Fig. 3. Steel cord produced by twisting two-wire strands around three-wire strands

Fig. 4. Cords held together by two knit yarns made from polyester.

Fig. 5. Cords held together by polyester and copper knits.

Fig. 6. Cross section of a typical specimen

Fig. 7. Load-deflection curve of specimen SF4.

Fig. 8. Field tests of SRP and FRP reinforced concrete Beams.

Fig. 9. Load-deflection relationships for concrete beams (field test)

Fig. 10. Geometry and dimensions of reinforced concrete beams employed in testing the effectiveness of SRG strengthening elements.

Fig. 11. Load-midspan deflection of reinforced concrete beams with and without SRG strengthening elements.

Fig. 12. Failure of SRG strengthened reinforced concrete beams.

Table 1: Properties of Epon 828 with Hardener HT-386

| **Specimen code** | **$E_m$** (ksi) | **$\nu_m$** | **Strength** (psi) | **$G_m$** (ksi) |
|---|---|---|---|---|
| **sp1** | 471 | 0.350 | 7163 | 175 |
| **sp2** | 460 | 0.380 | 8527 | 167 |
| **sp3** | 439 | 0.362 | 7460 | 161 |
| **sp4** | 408 | 0.341 | 7947 | 152 |
| **Average** | 444 | 0.358 | 7774 | 164 |

Table 2: Specimens Used in Experiments

| **Specimen Code** | **Angle of load-to-cords direction** (deg) | **Width** (in) | **Length** (in) | **Thickness** (in) | **Test Type** |
|---|---|---|---|---|---|
| **SLT1-5** | 0 | 1.0 | 12.0 | 0.25 | Tension |
| **STT1-5** | 90 | 1.0 | 7.0 | 0.25 | Transverse Tension |
| **STC1-5** | 90 | 0.5 | 5.5 | 0.25 | Transverse Compression |
| **SLC1-1** | 0 | 0.5 | 5.5 | 0.25 | Compression |
| **S45_1-3** | 45 | 1.0 | 10.0 | 0.25 | Tension (For shear modulus) |

Table 3. Results of Longitudinal Tension Tests

| **Specimen code** | **$E_{1c}$** (Msi) | **$E_{1w}$** (Msi) | **$E_{1cs}$** (Msi) | **$\nu_{12}$** | **$F_c$** (ksi) | **$F_w$** (ksi) | **$F_{cs}$** (ksi) | **Notes** |
|---|---|---|---|---|---|---|---|---|
| **SLT1-1** | 19.5 | 25.4 | 6.8 | 0.273 | 319 | 417 | 112 | |
| **SLT1-2** | 23.3 | 30.5 | 8.1 | 0.329 | 342 | 447 | 118 | |
| **SLT1-3** | 22.0 | 28.8 | 7.8 | 0.409 | 276 | 361 | 98 | **Failure at grip** |
| **SLT1-4** | 23.2 | 30.4 | 8.3 | 0.373 | 343 | 449 | 123 | |
| **SLT1-5** | 23.0 | 30.1 | 8.4 | 0.468 | 340 | 445 | 124 | |
| **Average** | 22.2 | 29.0 | 7.9 | 0.370 | 324 | 423.8 | 115 | |
| **Average w/o SLT3** | | | | | 336 | 440 | 119 | |
| **Average w/o SLT1 and SLT3** | 22.9 | 29.9 | 8.2 | 0.395 | 342 | 447 | 122 | |

Table 4. Results of Longitudinal Compression Tests

| **Specimen code** | **$E_{1c}$ (**Msi**)** | $E_{1w}$ (Msi) | **$E_{1cs}$** (Msi) | **$\nu_{12}$** |
|---|---|---|---|---|
| **SLC1** | 34.4 | 45.0 | 12.0 | 0.407 |
| **SLC2** | 33.3 | 43.6 | 12.0 | 0.246 |
| **SLC3** | 27.8 | 36.4 | 9.8 | 0.427 |
| **SLC4** | 36.6 | 47.9 | 12.6 | 0.468 |
| **Average** | 32.6 | 42.6 | 11.4 | 0.387 |

Table 5. Results of Transverse Tension Tests

| **Specimen code** | **$E_2$** (Msi) | **$\nu_{21}$** | **Strength** (psi) |
|---|---|---|---|
| **STT1** | 1.19 | 0.065 | 2354 |
| **STT2** | 0.74 | 0.045 | 2178 |
| **STT3** | 0.58 | 0.040 | 2193 |
| **STT4** | 0.83 | 0.034 | 2178 |
| **STT5** | 0.91 | 0.050 | 2193 |
| **Average** | 0.85 | 0.047 | 2219 |

Table 6. Results of Transverse Compression Tests

| **Specimen code** | **$E_2$** (Msi) | **$\nu_{21}$** | **Strength** (psi) |
|---|---|---|---|
| **STC1** | 0.86 | 0.042 | -8693 |
| **STC2** | 1.65 | 0.037 | -9012 |
| **STC3** | 0.93 | 0.026 | -10356 |
| **STC4** | 0.77 | 0.033 | -9620 |
| **STC5** | 1.97 | 0.023 | -8389 |
| **Average** | 1.24 | 0.032 | -9214 |

Table 7. Results of Tensile Tests Conducted with Loading Oriented at $45^o$ Relative to the Cords

| **Specimen code** | **$E_{45}$** (Msi) | **$G_{12}$** (Msi) |
|---|---|---|
| **S45_1** | 0.90 | 0.31 |
| **S45_2** | 0.95 | 0.33 |
| **S45_3** | 0.92 | 0.32 |
| **Average** | 0.92 | 0.32 |

Table 8. Comparison of Mechanical Properties Obtained Experimentally to Theoretical Predictions Based on Micromechanics

| | **Experimental Results** | **Analytical Results** | **Analytical Results 2*** |
|---|---|---|---|
| $E_1(ksi)$ **Tension** | 8159 | 8397 | |
| $E_1(ksi)$ **Compress.** | 11400 | 11826 | |
| $E_2(ksi)$ **Tension** | 849 | 605 | 910 |
| $E_2(ksi)$ **Compress.** | 1240 | 606 | 914 |
| $\nu_{12}$ **Tension** | 0.395 | 0.342 | |
| $\nu_{12}$ **Compress.** | 0.380 | 0.342 | |
| $\nu_{21}$ **Tension** | 0.047 | 0.041 | |
| $\nu_{21}$ **Compress.** | 0.032 | 0.026 | |
| $G_{12}(ksi)$ | 320 | 223 | 336 |

**Note**: * Analytical Results 2 were obtained from the *improved mechanics of materials.* The results for the in-plane shear modulus were identical in tension and compression.

Table 9. Specimens Used in Flexural Tests

| **Specimen code** | **Thickness** (in) | **Width** (in) | **Span** (in) | **Actual span** (in) | **Testing crosshead rate** (in/min) |
|---|---|---|---|---|---|
| **SF1** | 0.193 | 0.652 | 3.2 | 3.202 | 0.0886 |
| **SF2** | 0.170 | 0.707 | 3.2 | 3.202 | 0.1002 |
| **SF3** | 0.189 | 0.769 | 3.2 | 3.202 | 0.0903 |
| **SF4** | 0.182 | 0.732 | 6.2 | 6.196 | 0.3520 |
| **SF5** | 0.182 | 0.639 | 6.2 | 6.196 | 0.3520 |

Table 10. Results of Flexural Tests: Flexural Strength

| **Specimen Code** | **Span** (in) | **Deflection at Max Load** (in) | **Max Load** (lb) | **Max Flexural Stress** (ksi) | **Adjusted Flexural Strength** (ksi) |
|---|---|---|---|---|---|
| **SF1** | 3.2 | 0.172 | 508 | 100.8 | 100.8 |
| **SF2** | 3.2 | 0.199 | 433 | 101.4 | 101.4 |
| **SF3** | 3.2 | 0.235 | 630 | 110.1 | 110.1 |
| **SF4** | 6.2 | 0.767 | 247 | 95.2 | 102.6 |
| **SF5** | 6.2 | 0.501 | 201 | 88.2 | 90.8 |
| **Average** | | | | | 101.1 |

Table 11. Effectiveness of SRP reinforcement in concrete beams (field test)

| | **$M_n$ (Analytical)** (ft-kip) | **$M_u$ (Experimental)** (ft-kip) |
|---|---|---|
| **Benchmark** | 11.3 | 13.8 |
| **SRP Reinforced** | 26.7 | 24.9 |
| **Increase** (%) | 136 | 80 |

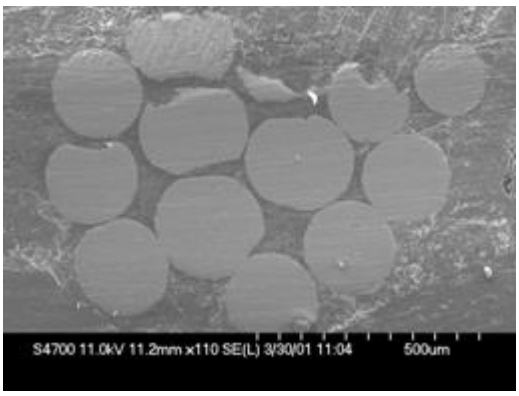

Fig. 1.

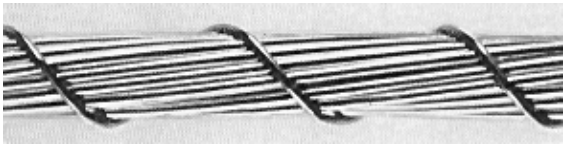
Fig. 2.

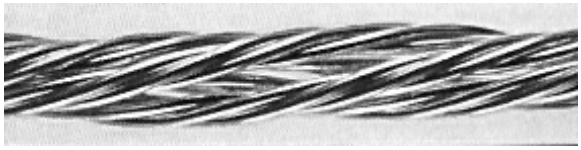
Fig. 3.

Fig. 4.

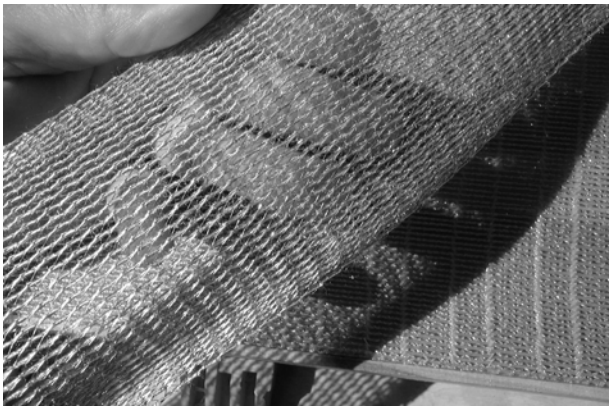

Fig. 5.

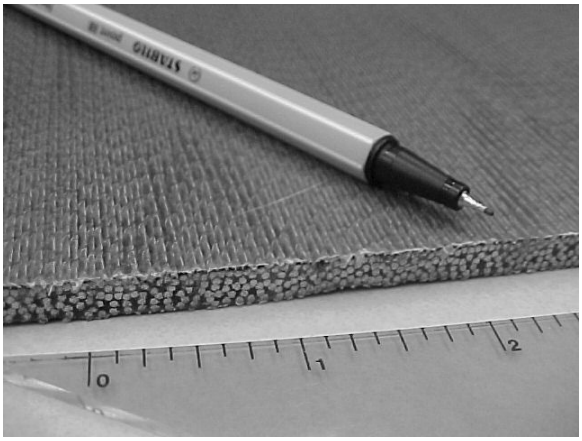


Fig. 6.

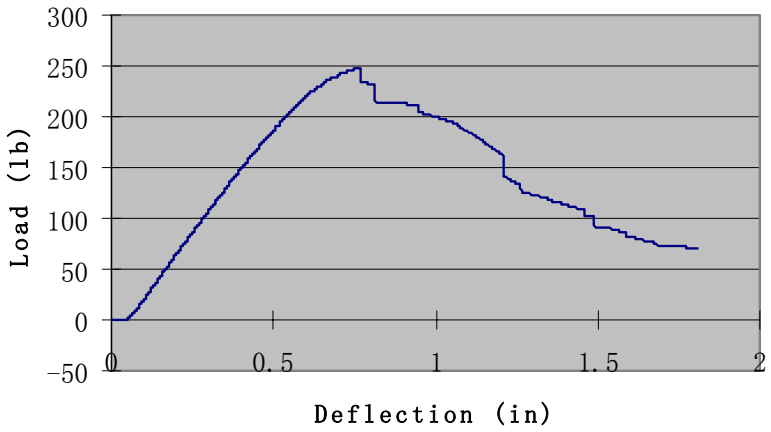
300
250
200
150
100
50
0
−50
Load (lb)
0
0.5
1
1.5
2
Deflection (in)

Fig. 7.

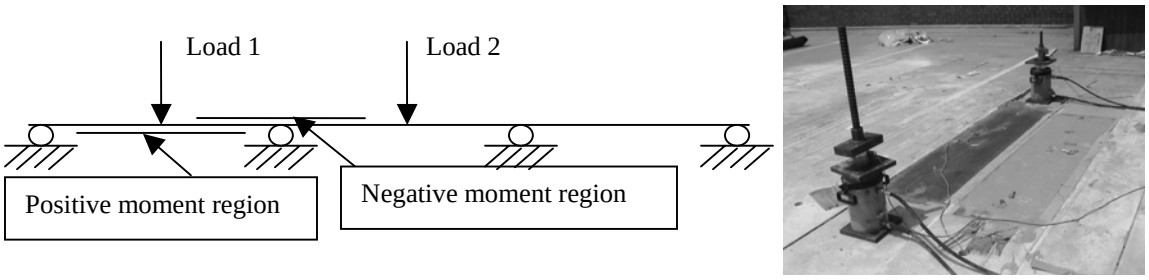
Load 1
Load 2
Positive moment region
Negative moment region

Fig. 8.

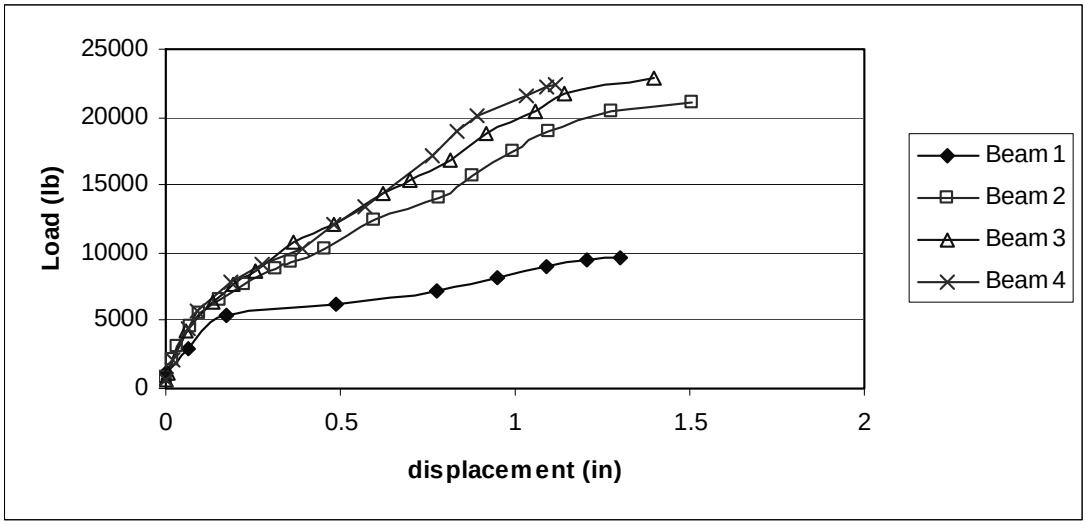
25000
20000
15000
10000
5000
0
Load (lb)
0
0.5
1
1.5
2
displacement (in)
Beam 1
Beam 2
Beam 3
Beam 4

Fig. 9

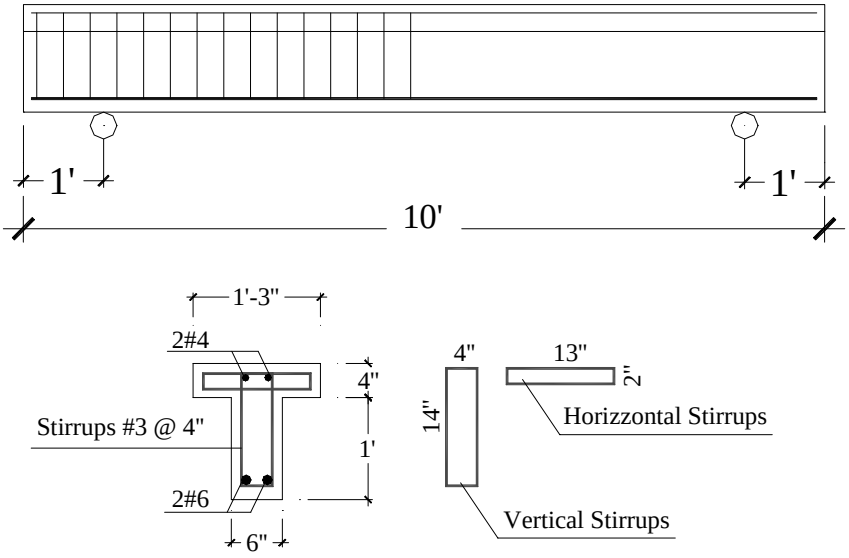
1'
1'
10'
1'-3"
2#4
4"
Stirrups #3 @ 4"
1'
2#6
6"
4"
13"
2"
14"
Horizzontal Stirrups
Vertical Stirrups

Fig. 10.

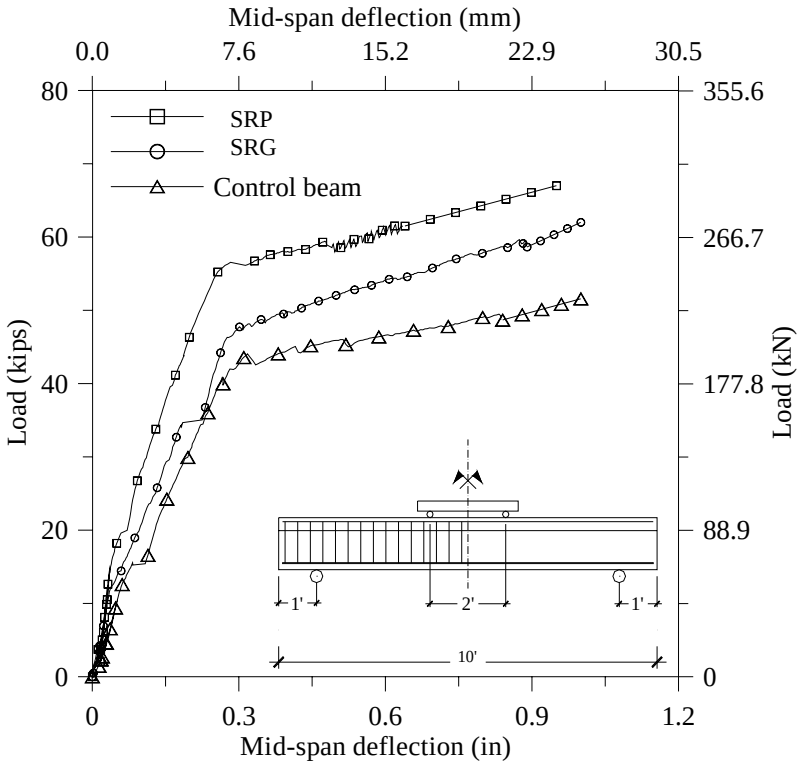


Fig. 11.

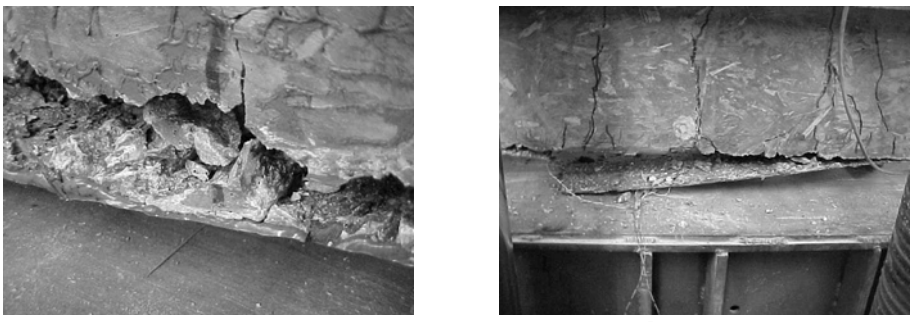

a) SRP b) SRG

Fig. 12.